J. Plasma Physics (2006), *vol.* 72, *part* 5, *pp.* 635–645. © 2006 Cambridge University Press
doi:10.1017/S002237780500396X First published online 28 February 2006 Printed in the United Kingdom

Neutron source from thin foil confined by two laser pulses

XIAOMEI ZHANG[1], BAIFEI SHEN[1], ZONGBAO FANG[1] and M. Y. YU[2]

[1]State Key Laboratory of High Field Laser Physics, Shanghai Institute of Optics and Fine Mechanics, PO Box 800-211, Shanghai 201800, People's Republic of China
[2]Theoretische Physik I, Ruhr-Universität Bochum, D-44780, Bochum, Germany
(dawnplum@163.com)

(Received 22 February 2005 and accepted 10 June 2005)

Abstract. Neutron production from a thin deuterium–tritium (D–T) foil irradiated by two intense femtosecond laser pulses from opposite sides with zero phase difference is studied analytically and numerically. For the interaction of a laser pulse of amplitude $a = 7$, focal area 100 μm^2 and areal density 4.4×10^{18} cm^{-2} with a D–T plasma foil, about 1.17×10^{21} neutron s^{-1} can be obtained, much more than from other methods. The profiles of the ion and electron densities are also calculated.

1. Introduction

Recent development of ultra-short ultra-intense laser pulses with focused intensities above 10^{18} W cm^{-2} has opened a new and rapidly progressing branch of relativistic plasma physics. The interaction of such intense laser pulses with plasmas of various densities is of great interest to many modern applications, such as compact electron accelerators [1–4], fast ignition in inertial fusion [5], and neutron generation [6–8]. A novel scheme for neutron production using available table-top lasers was proposed by Ditmire et al. [9]. When an intense femtosecond laser pulse interacts with a deuterium cluster, the atoms are ionized. The resulting electrons fly off rapidly, leaving the ions behind and an intense space-charge field is created. The Coulomb explosion that follows causes the deuterium ions to gain high kinetic energies and fusion reaction occurs when they collide. Collisions of the deuterium ions initiate the ^{2}H(d,n)^{3}He reaction, yielding neutrons [8]. About 10^4 neutrons per shot, or 10^5 per joule of laser energy, were produced. The neutron yield from laser-driven Coulomb explosion of clusters depends on the cluster size, the ion energy can be as high as 10 keV. In the more classical schemes of neutron production from the interaction of the intense laser pulse with plasma, excessive numbers of energetic electrons, photons and ions are produced. These energetic particles can cause nuclear reaction on the material around the target and produce undesirable background neutrons. Up to now, neutrons produced by thermonuclear reactions in ultra-short pulse plasma have been observed for low average plasma density, namely of the order of and below the critical value. There have been observations and simulations of neutron generation by the interaction of intense sub-picosecond laser pulses with underdense deuterium plasmas. For example, for an input laser energy of 62 J,

https://doi.org/10.1017/S002237780500396X Published online by Cambridge University Press

about $(1.0 \pm 0.2) \times 10^6$ neutrons with a mean kinetic energy of (2.5 ± 0.2) MeV were detected by Fritzler et al. [10].

However, the ion density in clusters is relatively low (underdense), but the fusion reaction rate is proportional to the square of the ion density. Thus, the concept of neutron production from the interaction of an intense laser pulse with *overdense* plasmas has received much recent attention. Volkov et al. [11] showed that the neutron number can be increased to 10^5 per joule of the incident laser energy, which is equal to that obtained in [9]. They reported neutron production by the ^{2}H(d,n)^{3}He reaction arising from illuminating a solid nanostructured target by femtosecond laser pulses of intensity 20 PW cm^{-2}. The target was structured by prior illumination with a laser pulse of similar intensity. For densities much larger than the critical density $n_c = 1.1 \times 10^{21}\ \lambda^2$ cm^{-3}, where the wavelength λ is in μm, most of the laser energy is reflected from the plasma surface in the case of normal incidence. For ultra-thin (thinner than the laser wavelength and plasma skin depth) foils, a large part of the laser pulse can penetrate the foil as an evanescent wave. Thus, the interaction of intense laser pulses with ultra-thin foils is of special interest [12–16].

Recently, we proposed an alternative method for producing neutrons from a frozen thin deuterium–tritium (D–T) foil plasma confined by intense laser fields [17]. In the laser confined fusion (LCF) approach, neutrons are produced by the fusion reaction D + T → He^4 (3.5 MeV) + n (14.1 MeV). The thin D–T foil is simultaneously illuminated by two circularly polarized laser pulses from opposite sides. The atoms are ionized rapidly and the electrons are pushed inward by the light pressure. The ions are then pulled inward by the space-charge field, but on a longer time scale. If the foil is not too thin, the ions need a long time to catch up with the electrons, so that their velocities will remain smaller than, but can be comparable to, the electron velocities. In the compressed quasi-stationary state, the ion density and temperature, which can be much larger than the electron temperature because of the large ion mass, can then be sufficiently large for a fusion reaction to occur. Clearly, such a compact neutron source based on LCF should be attractive for many modern applications.

In this paper, we consider the LCF concept in more detail, and in particular study the effect of the areal density of the target. We choose a not-too-thin frozen D–T (50% of each) foil. The number N of neutrons produced in the plasma is proportional to the square of the deuteron or tritium density $n_{\mathrm{D,T}}$

$$N \approx 0.25 n_{\mathrm{D}}^2 (\overline{\sigma v})_{\mathrm{DT}} V \tau, \tag{1.1}$$

where τ is the lifetime of the dense plasma or the time of its cooling, V is the plasma volume and $(\overline{\sigma v})_{\mathrm{DT}}$ is the thermonuclear reaction rate averaged over the Maxwellian distribution [18].

The number of neutrons produced depends strongly on the ion temperature and density. To maximize neutron production, in the LCF we propose to use a frozen D–T foil simultaneously illuminated from opposite sides by two circularly polarized laser pulses. For simplicity, we assume that the phase difference of the two laser pulses is zero. In general, this configuration leads to an unstable interaction [19]. However, if the foil is not too thin, the interaction can continue for a sufficiently long time for effective neutron production. In fact, in the simulations we did not find any observable modification of the foil during the main neutron production stage. By using a suitable pulse front, one can also achieve a quasi-stationary state with

https://doi.org/10.1017/S002237780500396X Published online by Cambridge University Press

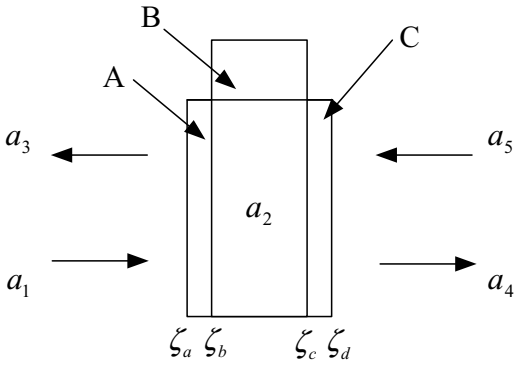


Figure 1. Schematic drawing of electron and ion densities of the foil, with ξ_a, ξ_b, ξ_c and ξ_d marking left and right layer boundaries. The wave amplitudes in the various regions are given by a_1, a_2, a_3, a_4 and a_5. Layer A is the layer where there are only ions and no electrons. Layer B is the layer where there are both ions and electrons.

the desired ion temperature. The present work is devoted to this quasi-stationary state of the interaction. Our analytical results are validated by one-dimensional (1D) particle-in-cell (PIC) simulations based on the code LPIC++ [20].

2. Theoretical analysis

Thin foils illuminated by a single laser pulse have been studied by many authors [14–16, 21, 22]. We consider a thin foil illuminated simultaneously by two circularly polarized laser pulses from opposite sides. This configuration has been studied in detail in [19, 23]. In [19], it was assumed that ions are fixed and electrons are cold [24–27]. In [23], it was assumed that the laser pulse is long enough for the ions to follow electron motion within the foil. The electron and ion densities are set to be equal, so that the electrostatic field is zero. Here we shall relax these assumptions, so that stationary solutions for different foil thicknesses can be considered.

We shall start with Maxwell's equations for the electromagnetic field and the relativistic equation of motion for the electrons, or

$$\nabla^2\mathbf{A} - \frac{1}{c^2}\frac{\partial^2\mathbf{A}}{\partial t^2} = \frac{4\pi e}{c}n\mathbf{u}, \tag{2.1}$$

$$\nabla^2\phi = 4\pi e(n_\mathrm{e} - n_\mathrm{i}) \tag{2.2}$$

and

$$\frac{d\mathbf{P}}{dt} = e\mathbf{E} + \frac{e}{c}(\mathbf{u}\times\mathbf{B}), \tag{2.3}$$

where $\mathbf{A}$ and ϕ are vector and scalar potentials satisfying the Coulomb gauge $\nabla\cdot\mathbf{A} = 0$, $\mathbf{E} = -(1/c)\partial\mathbf{A}/\partial t$ and $\mathbf{B} = \nabla\times\mathbf{A}$, n_e and n_i are electron and ion density, respectively, e is the charge of an electron and c is the light speed in vacuum. As long as the laser spot size is much larger than the depth of laser penetration, one can assume planar geometry.

The foil and field configuration considered here is sketched in Fig. 1. It shows that the light pressure of the incident waves a_1 and a_5 compresses the electrons and the ions inside the foil such that the electron layer extends from ξ_b to ξ_c and the ion layer extends from ξ_a to ξ_d. There are three main regions in the foil: both ions and electron

https://doi.org/10.1017/S002237780500396X Published online by Cambridge University Press

exist in B, and only ions exist in A and C because the much heavier ions are unable to follow the electrons. The incident and reflected plane waves are represented by the constant amplitudes a_1, a_5 and a_3, a_4, respectively. In the present analytical model, only the evanescent waves in the overdense layer create a field with space-dependent amplitude $a_2(\xi)$ and phase $\theta(\xi)$, the corresponding values at the left and the right boundaries are a_b, a_c, θ_b and θ_c, respectively. From (2.3) we obtain the stationary conservation equations for the electrons and the ions.

2.1. The central plasma layer

In this layer both electrons and ions exist. The ponderomotive force of the laser field is balanced by the electron thermal pressure force and the electrostatic forces on the electrons and ions. One then obtains

$$N_{\mathrm{e}}\frac{\partial\gamma}{\partial\xi} = N_{\mathrm{e}}\frac{\partial\psi}{\partial\xi} - T_{\mathrm{e}}\frac{\partial N_{\mathrm{e}}}{\partial\xi}, \tag{2.4}$$

$$N_{\mathrm{i}}\frac{\partial\psi}{\partial\xi} = -T_{\mathrm{i}}\frac{\partial N_{\mathrm{i}}}{\partial\xi}, \tag{2.5}$$

where

$$u = a/\gamma, \tag{2.6}$$

$\gamma = (1 + a^2)^{1/2}$, $a = eA/mc^2$, $\xi = \omega_{\mathrm{L}} z/c$, $\psi = e\phi/mc^2$, m is the electron mass, ω_{L} is the laser frequency, $N_{\mathrm{i}} = n_{\mathrm{i}}/n_c$ and $N_{\mathrm{e}} = n_{\mathrm{e}}/n_c$ are the normalized ion and electron densities, respectively, and n_c is the critical electron density. From (2.4) and (2.5) we easily obtain the ion density

$$N_{\mathrm{i}} = N_0' \exp(-\gamma/T_{\mathrm{i}}) N_{\mathrm{e}}^{-T_{\mathrm{e}}/T_{\mathrm{i}}}. \tag{2.7}$$

It follows that

$$N_{\mathrm{i}} = N_0' \exp(-\gamma/T_{\mathrm{i}}) \quad \text{for} \quad T_{\mathrm{e}} \ll T_{\mathrm{i}}, \tag{2.8}$$

$$N_{\mathrm{e}} = N_0' \exp(-\gamma/T_{\mathrm{e}}) \quad \text{for} \quad T_{\mathrm{i}} \ll T_{\mathrm{e}}. \tag{2.9}$$

Case (2.9) was discussed in [23], so here we shall only discuss the case of cold electrons ($T_{\mathrm{e}} \ll T_{\mathrm{i}}$).

Taking the field $a = a_0(\xi)\exp(i\omega t + i\theta(\xi))$ with real amplitude $a_0(\xi)$ and real phase $\theta(\xi)$, and substituting it into (2.1) and (2.2) and connecting with (2.8) we obtain two constants of motion with respect to ξ,

$$M = -\frac{\partial\theta}{\partial\xi}(\gamma^2 - 1) = -\frac{\partial\theta}{\partial\xi}a^2, \tag{2.10}$$

$$\begin{aligned} W &= \frac{1}{2a^2}\left(\frac{\partial\gamma}{\partial\xi}\right)^2 + \frac{M^2}{2a^2} + \frac{\gamma^2}{2} + T_{\mathrm{i}}N_{\mathrm{i}} \\ &= \frac{1}{2(a^2+1)}\left(\frac{\partial a}{\partial\xi}\right)^2 + \frac{a^2+1}{2} + T_{\mathrm{i}}N_{\mathrm{i}}. \end{aligned} \tag{2.11}$$

where M the net flow of the laser pulse and for the case of two similar laser pulses,

https://doi.org/10.1017/S002237780500396X Published online by Cambridge University Press

$M = 0$. From (2.11) we obtain

$$\frac{\partial^2 \gamma}{\partial \xi^2} = N_{\rm i}\gamma^2 - 2\gamma^3 + \gamma + 2W\gamma - 2T_{\rm i}N_{\rm i}\gamma - N_{\rm i}, \tag{2.12}$$

and then we obtain the electron density,

$$\begin{aligned} N_{\rm e} &= \frac{\partial^2 \gamma}{\partial \xi^2} + N_{\rm i} \\ &= \gamma + 2W\gamma - 2\gamma^3 + (\gamma^2 - 2T_{\rm i}\gamma)N_{\rm i} \\ &= \sqrt{a^2+1}(2W - 2a^2 - 1) + (a^2 + 1 - 2\sqrt{a^2+1}\,T_{\rm i})Ni, \end{aligned} \tag{2.13}$$

using (2.2).

2.2. The ion layers

In the ion layers A and C, the electrostatic pressure is balanced by the ion thermal pressure, so that

$$N_{\rm i}\frac{\partial \psi}{\partial \xi} = -T_{\rm i}\frac{\partial N_{\rm i}}{\partial \xi},$$

and (2.2) becomes

$$\frac{\partial^2 \psi}{\partial \xi^2} = -N_{\rm i}. \tag{2.14}$$

We then obtain for the ion density

$$N_{\rm i} = N_0 \sec^2\left(\sqrt{\frac{N_0}{2T_{\rm i}}}\xi\right) \tag{2.15}$$

in layers A and C.

Invoking the continuity of the transverse electric ($E = -\partial a/\partial t$) and magnetic ($B = \partial a/\partial \xi$) fields at the boundaries between the layers, we find

$$2(a_1^2 + a_3^2) = (\partial a_b/\partial \xi)^2 + M^2/a_b^2 + a_b^2, \tag{2.16}$$

$$M = a_1^2 - a_3^2, \tag{2.17}$$

at ξ_b (left boundary). For $M = 0$, (2.16) becomes

$$(\partial a_b/\partial \xi)^2 + a_b^2 = 4a_1^2. \tag{2.18}$$

In the layer avoiding electrons we can obtain the constant

$$\begin{aligned} W &= \frac{\gamma^2}{2a^2}\left(\frac{\partial \gamma}{\partial \xi}\right)^2 + \frac{M^2}{2a^2} + \frac{\gamma^2}{2} \\ &= \frac{1}{2}\left(\frac{\partial a}{\partial \xi}\right)^2 + \frac{a^2+1}{2} \\ &= 2a_1^2 + \frac{1}{2}, \end{aligned} \tag{2.19}$$

and accordingly we obtain

$$a = 2a_1 \sin\left[\pm\xi + \arcsin\left(\frac{a_0}{2a_1}\right)\right] \tag{2.20}$$

for the electrostatic field.

https://doi.org/10.1017/S002237780500396X Published online by Cambridge University Press

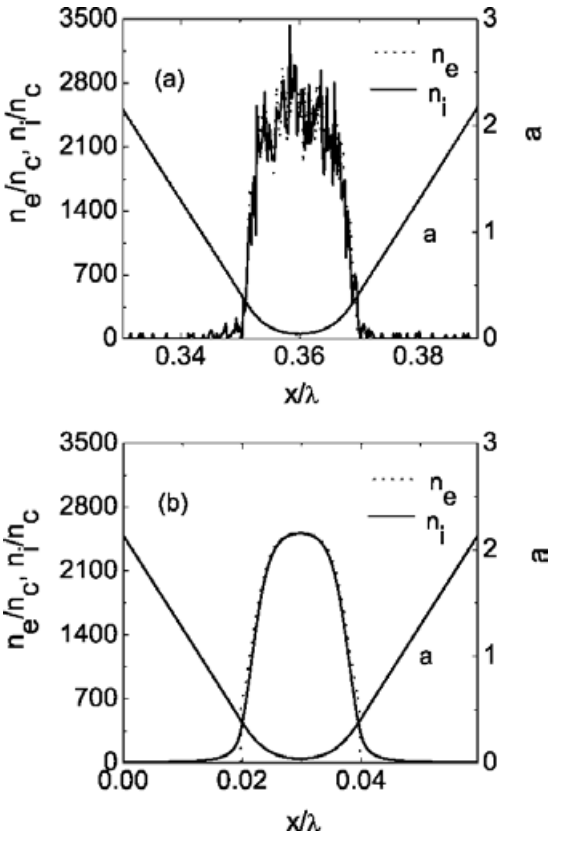


Figure 2. The electron and ion density profiles n_e, n_i and the laser field a as functions of the foil depth x/λ. Two circularly polarized laser pulses of amplitude $a = 7$ and phase difference $\phi_{51} = 0$ illuminate the foil from opposite sides. The electron density per unit area of the foil is 4.4×10^{18} cm^{-2}. (a) Simulation result when a stationary state is reached. (b) Analytical results.

The next task is to obtain the constant W, the space-dependent laser field and the ion or electron densities in terms of the amplitudes a_1, a_5, the ion temperature and the foil areal density. From (2.19) and (2.11), one can then obtain W. We rewrite (2.20) and (2.12) as

$$\frac{\partial a}{\partial \xi} = \pm\sqrt{4a_1^2 - a^2}, \tag{2.21}$$

$$\frac{\partial a}{\partial \xi} = \pm\sqrt{(2W - a^2 - 1 - 2T_i N_i)(a^2 + 1)}. \tag{2.22}$$

Using (2.15), (2.20), (2.21), (2.8), (2.13) and (2.22), one can calculate the laser field and ion or electron density as a function of space. In the analytical calculation, $a(\xi_a)$ at the left-hand boundary is found by trial and error, such that the desired self-consistent ion density $N_i(\xi_a)$ (= 10 in the present example) at the left-hand boundary is realized.

https://doi.org/10.1017/S002237780500396X Published online by Cambridge University Press

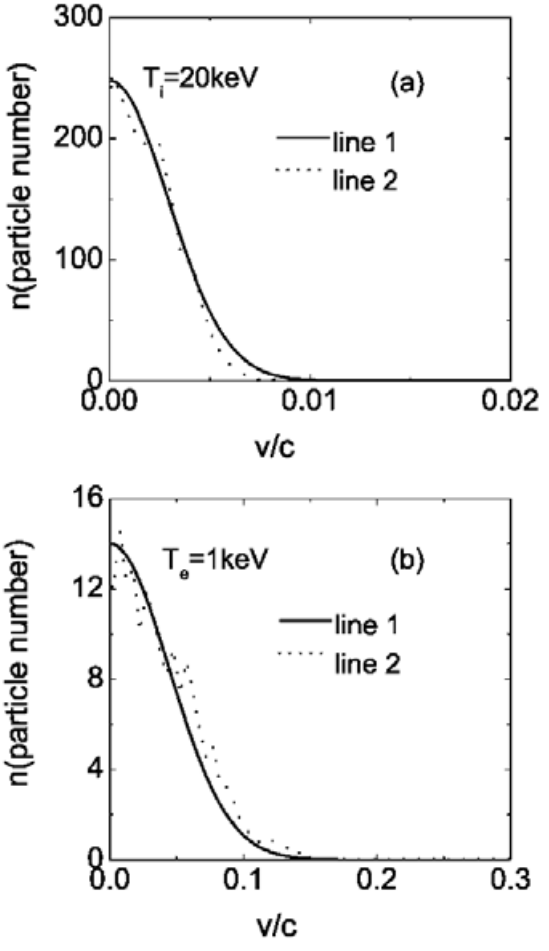


Figure 3. The ion and electron temperature profiles after compression. The areal plasma density of the foil is 4.4×10^{18} cm^{-2}. Lines 1 and 2 are the analytical and simulation results, respectively.

3. Results

We give the results for a thin D–T foil with an areal plasma density of 4.4×10^{18} cm^{-2} illuminated by two circularly polarized laser pulses of intensity 0.67×10^{20} W cm^{-2} ($a = 7$) and wavelength 1 μm. The initial relative phase between the two laser pulses is zero, i.e. $\phi_{51} = 0$. In the PIC simulation, the ion charge-to-mass ratio is $q/e = 1$ and the ion mass is 2.5 times the proton mass, or $m_{\rm i}/m_{\rm e} = 4590$, which is the average mass of the deuterium and tritium ions. The pulse length is 400 laser periods.

In Fig. 2(a), we show the profiles of the electron and ion densities as well as the laser field after a stationary state is reached in the 1D PIC simulation. The analytical result is given in Fig. 2(b). The initial conditions for the theory and simulation are the same. The temperature used in the analytical calculation is $T_{\rm e} = 0$ keV and $T_{\rm i} = 0.039 m_{\rm e} c^2 = 20$ keV, which is taken from the PIC simulation. The foil thickness is compressed to $0.016\,\mu$m and the laser field inside the foil

https://doi.org/10.1017/S002237780500396X Published online by Cambridge University Press

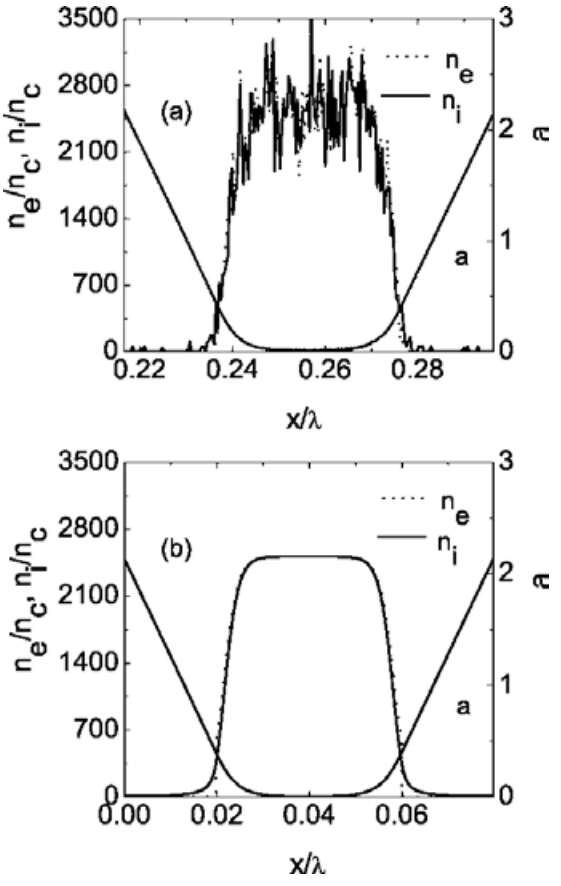


Figure 4. Same as in Fig. 2, but for areal density 9.9×10^{18} cm^{-2}.

tends to zero ($a = 0.04$). The ion density is about $n_i = 2400 n_c$, corresponding to $10.96\,\mathrm{g\,cm^{-3}}$. The ion mass density is still much smaller ($200\,\mathrm{g\,cm^{-3}}$) than in inertial confined fusion (ICF). Nevertheless, it is much larger than that in clusters or underdense plasmas [9, 10]. The reaction rate $(\overline{\sigma v})_{\mathrm{DT}}$ is $4.2 \times 10^{-16}\,\mathrm{cm^{-3}\,s^{-1}}$ for $T_i = 20$ keV. Using (1.1), one can compute the number of neutrons generated. For two femtosecond laser pulses each with a focal area of $10 \times 10\ \mu\mathrm{m}^2$, we can obtain 1.17×10^{21} neutrons per second or about 10^8 neutrons per shot. From the electron and ion velocities of the simulation, we can calculate the corresponding temperature profiles as shown in Fig. 3. Thus, we have $T_i = 20$ keV and $T_e = 1$ keV. We see that the assumption $T_i \gg T_e$ is well satisfied.

The results for a thicker D–T foil of areal plasma density 9.9×10^{18} cm^{-2} are given in Fig. 4. We find that after compression the plasma density is almost similar to that of the preceding case but its final thickness is about $0.0375\ \mu$m, which is thicker than that of the preceding case. From Fig. 4, we see that because of the larger thickness, the laser field inside the foil is smaller ($a = 0.002$) than that of the case in Fig. 2. Since the total ion number has increased because of the larger plasma volume, more neutrons can be produced at the expense of more laser energy being needed to compress the thicker D–T foil. In general, given the laser parameters, one can easily find the optimum foil thickness.

https://doi.org/10.1017/S002237780500396X Published online by Cambridge University Press

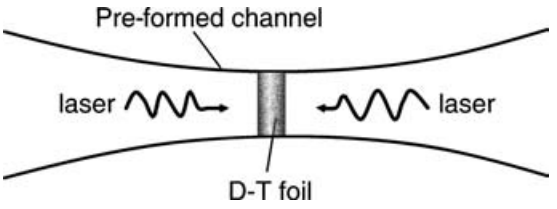


Figure 5. Schematic drawing of a foil placed inside a pre-formed channel.

In the stationary state, the ion density is mainly determined by the ion temperature and the laser intensity, and is almost independent of the areal density of the foil. The largest ion density at the center (where the laser field is nearly zero) is

$$N_{\mathrm{i}}^{\max} \sim \frac{2a^2}{T_{\mathrm{i}}} \tag{3.1}$$

for a thick foil. For a laser pulse of $a = 7$ and ion temperature $T_{\mathrm{i}} = 20$ keV, we have $N_{\mathrm{i}}^{\max} = 2499$, which is in excellent agreement with the simulation result.

The total number of neutrons per shot may be increased by increasing the pulse energy or the plasma volume. Increasing the ion temperature also seems to be an efficient way of obtaining more neutrons, since the reaction rate would be increased. However, the ion density would then decrease. For example, the reaction rate would be about four times smaller if the ion temperature were 10 keV (instead of 20 keV). Since in this case the ion density would be increased, the total number of neutrons produced may not changed significantly, although the process is more efficient for lower ion temperatures. We found that an ion temperature of between 10 and 20 keV is optimum for neutron production in the laser-compressed D–T foil plasma.

4. Conclusions

In conclusion, we have introduced a new method for producing controllable quantities of neutrons as well as a simple analytical model for it. Using the cold-electron steady-state model we have obtained analytical solutions for the problem of the compression of a thin D–T foil from both sides by circularly polarized lasers. The foil is represented by a dense plasma containing free electrons and ions. We find that 1.17×10^{21} neutrons per second are produced from the interaction of two femtosecond laser pulses of amplitude 0.67×10^{20} W cm^{-2} and focal area 10×10 μm^2 with a thin D–T foil of areal plasma density 4.4×10^{18} cm^{-2}. We have not considered the case when the electron temperature is comparable to the ion temperature. This case is expected to be of lower efficiency because of the lower achievable ion density, and the plasma will expand under the two thermal pressures.

The scheme introduced here can also be useful for producing other elementary particles. Because of its compactness, it should be of much interest for applications in nuclear physics, materials science as well as other fields.

The important question of foil stability in two and three dimensions is beyond the scope of the present paper. Both the PIC simulations and the analytical model here are 1D and are expected to be valid if the focusing area is sufficiently large. In real experiments, the fusion material can also be placed inside a preformed channel, as shown in Fig. 5, so that the plasma can be tightly confined. One can also accelerate

https://doi.org/10.1017/S002237780500396X Published online by Cambridge University Press

the foil as a whole using light pressure [28, 29] and place it inside a pre-formed channel.

References

[1] Malka G. et al. 1997 Suprathermal electron generation and channel formation by an ultrarelativistic laser pulse in an underdense preformed plasma. *Phys. Rev. Lett.* **79**, 2053.

[2] Pukhov, A., Sheng, Z. M. and Meyer-ter-Vehn, J. 1999 Particle acceleration in relativistic laser channels. *Phys. Plasmas* **6**, 2847.

[3] Gahn, C., Tsakiris, G. D., Pukhov, A., Meyer-ter-Vehn, J., Pretzler, G., Thirolf, P., Habs, D. and Witte, K. J. 1999 Multi-MeV electron beam generation by direct laser acceleration in high-density plasma channels. *Phys. Rev. Lett.* **83**, 4772.

[4] Pukhov A. and Meyer-ter-Vehn, J. 1996 Relativistic magnetic self-channeling of light in near-critical plasma: three-dimensional particle-in-cell simulation. *Phys. Rev. Lett.* **76**, 3975.

[5] Tabak, M., Hammer, J., Glinsky, M. E., Kruer, W. L., Wilks, S. C., Woodworth, J., Campbell, E. M., Perry, M. D. and Mason, R. J. 1994 Ignition and high gain with ultrapowerful lasers. *Phys. Plasmas* **1**, 1626.

[6] Pretzler, G., Saemann, A. and Pukhov, A. 1998 Neutron production by 200 mJ ultrashort laser pulses. *Phys. Rev.* E **58**, 1165.

[7] Norreys, P. A., Fews, A. P. and Begg, F. N. 1998 Neutron production from picosecond laser irradiation of deuterated targets at intensities of 10^{19} W cm^{-2}. *Plasma Phys. Control. Fusion* **40**, 175.

[8] Zweiback, J., Smith, R. A. and Cowan, T. E. 2000 Nuclear fusion driven by Coulomb explosions of large deuterium clusters. *Phys. Rev. Lett.* **84**, 2634.

[9] Ditmire, T., Zweiback, J., Yanovsky, V. P., Cowan, T. E., Hays, G. and Wharton, K. B. 1999 Nuclear fusion from explosions of femtosecond laser-heated deuterium clusters. *Nature* **398**, 489.
Ditmire, T. 1998 Simulation of exploding clusters ionized by high-intensity femtosecond laser pulses. *Phys. Rev.* A **57**, R4094.

[10] Fritzler, S., Najmudin, Z., Malka, V., Krushelnick, K., Marle, C., Walton, B., Wei, M. S., Clarke, R. J. and Dangor, A. E. 2002 Ion heating and thermonuclear neutron production from high-intensity subpicosecond laser pulses interacting with underdense plasmas. *Phys. Rev. Lett.* **89**, 165004.

[11] Volkov, R. V., Golishnikov, D. M., Gordienko, V. M., Mikheev, P. M., Savel'ev, A. B., Sevast'yanov, V. D., Chernysh, V. S. and Chutko, O. V. 2000 Neutron generation in dense femtosecond laser plasma of a structured solid target. *JETP Lett.* **72**, 402.

[12] Guerin, S., Mora, P., Adam, J. C., Heron, A. and Laval, G. 1996 Propagation of ultraintense laser pulses through overdense plasma layers. *Phys. Plasmas* **3**, 2693.

[13] Forsman, A., Ng, A. and Chiu, G. 1998 Interaction of femtosecond laser pulses with ultrathin foils. *Phys. Rev.* E **58**, 1248.

[14] Vshivkov, V. A., Naumova, N. M., Pegoraro, F. and Bulanov, S. V. 1998 Nonlinear electrodynamics of the interaction of ultra-intense laser pulses with a thin foil. *Phys. Plasmas* **5**, 2727.

[15] Giulietti, D. et al. 1997 Observation of solid-density laminar plasma transparency to intense 30 femtosecond laser pulses. *Phys. Rev. Lett.* **79**, 3194; Teychenne, D., Giulietti, A., Giulietti, D. and Gizzi, L. A. 1998 Magnetically induced optical transparency of overdense plasmas due to ultrafast ionization. *Phys. Rev.* E **58**, R1245.

[16] Fuchs, J. et al. 1998 Transmission through highly overdense plasma slabs with a subpicosecond relativistic laser pulse. *Phys. Rev. Lett.* **80**, 2326.

[17] Shen, B., Zhang, X. and Yu, M. Y. 2005 Laser-confined fusion. *Phys. Rev.* E **71**, 015401(R).

https://doi.org/10.1017/S002237780500396X Published online by Cambridge University Press

[18] Brakner, K. and Jorna, S. 1977 *Laser Driven Fusion*. Moscow: Atomizdat (also KMS Fusion, 1973).

[19] Shen, B. and Meyer-ter-Vehn, J. 2001 High-density ($>10^{23}$ cm^3) relativistic electron plasma confined between two laser pulses in a thin foil. *Phys. Plasmas* **8**, 1003.

[20] Lichters, R., Pfund, R. W. and Meyer-ter-Vehn, J. 1997 Computer code `LPIC++` Report MPG225, MPI Quantenoptik, Garching.

[21] Guerin, S., Mora, P., Adam, J. C., Heron, A. and Laval, G. 1996 Propagation of ultraintense laser pulses through overdense plasma layers. *Phys. Plasmas* **3**, 2693.

[22] Forsman, A., Ng, A. and Chiu, G. 1998 Interaction of femtosecond laser pulses with ultrathin foils. *Phys. Rev.* E **58**, 1248.

[23] Shen, B. and Meyer-ter-Vehn, J. 2002 Pair and γ-photon production from a thin foil confined by two laser pulses. *Phys. Rev.* E **65**, 016405.

[24] Sudan, R. N. 1993 Mechanism for the generation of 10^9 G magnetic fields in the interaction of ultraintense short laser pulse with an overdense plasma target. *Phys. Rev. Lett.* **70**, 3075.

[25] Lai, C. S. 1976 Strong transverse electromagnetic waves in overdense plasmas. *Phys. Rev. Lett.* **36**, 966.

[26] Kaw, P. and Dawson, J. 1970 Relativistic nonlinear propagation of laser beams in cold overdense plasmas. *Phys. Fluids* **13**, 472.

[27] Max, C. and Perkins, F. 1971 Strong electromagnetic waves in overdense plasmas. *Phys. Rev. Lett.* **27**, 1342.

[28] Shen, B. and Xu, Z. 2001 Transparency of an overdense plasma layer. *Phys. Rev.* E **64**, 056406.

[29] Esirkepov, T., Borghesi, M., Bulanov, S. V., Mourou, G. and Tajima, T. 2004 Highly efficient relativistic-ion generation in the laser-piston regime. *Phys. Rev. Lett.* **92**, 175003.

https://doi.org/10.1017/S002237780500396X Published online by Cambridge University Press